



Progressive deformation and failure mechanism of loess fill slopes induce by rainfall: insights from flume model tests

Xingsheng Lu^{1,3,4} · Yao Jiang^{1,2,4} · Nianqin Wang³ · Huihui Shen⁵

Received: 7 May 2023 / Accepted: 8 September 2023 / Published online: 20 September 2023
© Springer-Verlag GmbH Germany, part of Springer Nature 2023

Abstract

In recent years, many hill flattening and gully filling projects are carried out in the northwest of China to create land for construction. These projects have formed a number of loess fill slopes, which are prone to failure induced by rainfall. However, the failure mechanism of loess fill slope is not clear under rainfall conditions. In this study, a flume model experiment is carried out to reveal the characteristics and mechanism of failure loess fill slopes. The volumetric water content, soil pressure, and pore water pressure are analyzed to investigate the effect of rainfall infiltration on fill slope. The results shown that rain-induced failure mode of loess fill slopes exhibited progressive multi-stage sliding characteristics, including slope toe failure, crack development and penetration, local sliding, and overall misaligned sliding stages. The influence of the weak interface between the fill slope and the bedrock/natural slope on slope damage was revealed based on the hydromechanical characteristics. It is shown that the maximum migration rate of wetting front along the weak interface is about 5 times that in loess fill, and the weak interface becomes the dominant channel controlling the hydrological characteristics of the slope, accelerating the saturation of the fill loess slope and generating seepage forces towards the outside of the slope, causing the loess fill slope prone to shear slide along with weak interface. Therefore, we believe that the weak interface between the fill slope and the bedrock/natural slope surface plays an important role in slope failure.

Keywords Loess fill slope · Flume model experiment · Failure mode · Failure mechanism

Introduction

In recent years, with the implementation of China's "Western Development" strategy and the "One Belt, One Road" initiative, a series of construction activities such as hill flattening and gully filling have been carried out in the loess

mountainous areas in northwest China to expand the urban land, and the number of loess fill slopes has increased sharply (Wang et al. 2018; Zhang et al. 2023). The stability of loess fill slope is determined by the site topographic condition, the compaction degree, water content, and the construction process and quality. However, owing to short construction time and large filling sites, the construction process of loess fill slope is difficult to meet the construction quality requirement, which results in large deformation such as differential post-construction settlement. More seriously, influenced by rainfall, the deformed loess fill slopes are prone to form the loess landslide easily, causing serious casualties and economic loess (Wang et al. 2014a, b; Zhang et al. 2014a, b; Deng et al. 2018; Wang et al. 2018; Chen and Zhang 2021). For example, in October 2009, a significant landslide occurred at Panzhuhua Airport, which had a stepped form. The incident was a result of inadequate treatment of weak foundations on the lower part of a high fill slope under rainfall conditions. The landslide caused the reactivation of an old landslide at Yijiaping below, resulting in substantial economic losses and airport disruptions (Wang et al. 2013). In April 2015, a nearly upright loess

✉ Yao Jiang
yjiang@imde.ac.cn

¹ Key Laboratory of Mountain Hazards and Earth Surface Processes, Institute of Mountain Hazards and Environment, Chinese Academy of Sciences, Chengdu 610299, China
² China–Pakistan Joint Research Center On Earth Sciences, CAS-HEC, Islamabad 45320, Pakistan
³ College of Geology and Environment, Xi'an University of Science and Technology, Xi'an 710068, China
⁴ University of Chinese Academy of Sciences, Beijing 100049, China
⁵ Sinochem General Administration of Geology and Mines, Shaanxi Institute of Geological Exploration, Xi'an 710065, China

high fill slope in Henan Province broke under rainfall conditions, burying 20 houses and causing direct economic losses of approximately 11 million (Chang et al. 2021). In July 2016, a stepped loess high fill slope in Yan'an, Shaanxi Province, collapsed during a period of heavy rainfall. The landslide resulted in a sliding volume of approximately 15.41 million m³ and led to substantial economic losses (Zhang 2020). In summary, fill loess landslides have become a major geologic disaster in loess areas of China, which posed a great threat to regional economic development and engineering construction. Therefore, it is urgent to reveal the evolutionary characteristics and failure mechanism of fill loess landslides for reducing the risk of fill loess landslides, disaster prevention, and prediction.

To study the process and mechanism of slope failure induced by rainfall, current research methods have mainly utilized numerical simulations (Tsai et al. 2008; Lee et al. 2009; Luca et al. 2014; Song et al. 2016; Regmi et al. 2017; Elkamhawy et al. 2018), in situ experiments (Lim et al. 1996; Zhang et al. 2000, 2013, 2022; Tu et al. 2009; Zhang et al. 2014a, b), and laboratory flume tests (Okura et al. 2002; Moriwaki et al. 2004; Cui et al. 2014; Wu et al. 2017). Numerical simulation has been widely adopted to investigate the hydrological process and characteristics of the slope, deformation evolution, and stability analysis of slope under rainfall condition (Cho 2016; Yang et al. 2018). Wang et al. (2014a, b) constructed the coupled equations of soil motion and rainfall seepage and proposed a two-level Lagrangian strain smoothing regularized meshfree formulation based on the stabilized conforming nodal integration for analyzing the rainfall infiltration triggered large deformation slope failure. Numerical results demonstrate that the present method is very effective for modeling large deformation slope failure processes induced by rainfall infiltration. In situ experiments are carried out on slopes using contact and non-contact monitoring instruments for long-term monitoring which mainly focused on the external variation characteristics of slope failure (Tu et al. 2009; Chen et al. 2019; Zhang et al. 2019a, b, c). Bentley et al. (2023) conducted a 5-year surface displacement monitoring program using UAV-based photogrammetry and conventional total station measurements of ground control marker grids on an 11-m-high slope to assess whether surface displacement measurements can serve as an indicator of potential expansion of a progressive failure surface. Based on this data, it can be concluded that sufficient pre-failure deformations exist in the case of episodically retrogressing landslides occurring in the Champlain Sea Clay within the urban boundary of the City of Ottawa, which can be measured and serve as precursors to progressive failure. Compared with numerical simulation and in situ experiments, laboratory flume tests are the most reliable method to study the failure mode and mechanism of landslides induced by rainfall. It has the advantages of easy control and observation, is not limited by environmental conditions, and can better reflect the influence of special factors on the experimental results (Wang and Sassa 2001; Rieke-Zapp and Nearing 2005; He et al. 2018; Guo et al.

2023). Consequently, Zhang et al. (2019a, b, c) carried out a series of laboratory flume tests to reveal the failure mode of slope under rainfall condition and analyzed the influence of rainfall characteristics on slope stability. Askarnejad et al. (2018) conducted a full-scale landslide-triggering experiment by artificial rainfall to analyze the landslide movement behavior. However, the weak interface between the loess fill slope and the bedrock/nature slope makes the fill slope with a distinctive sloping geological structure. This particular geological formation serves to diminish the cohesion between the filled slope and the nature slope, and consequently, increases the rainwater infiltration rate of the fill loess slope. Therefore, in contrast to uniform loess slopes, the instability mechanism of filled loess slopes is significantly more complex and the related research results are fewer and not deep enough (Zhang et al. 2013; Wang et al. 2019). For example, Zhang et al. (2019a, b, c) and Chang et al. (2021) conducted a preliminary analysis of the failure characteristics, failure mode and early warning model construction of fill slopes under rainfall conditions by using flume tests, which revealed the relationship between external factors (rainfall intensity, surface morphology of loess fill slopes) and slope failure. However, the study did not consider the influence of the special weak interfaces of the fill slopes on the seepage, stress, and failure characteristics. Guo et al. (2023) illustrated the influence of weak interfaces on seepage characteristics, stress characteristics, and deformation characteristics of the fill slope, and confirmed that weak interfaces are the main factors affecting the failure characteristics of fill slopes. However, the failure mechanism of fill slope under the influence of weak interface is not clear.

In this study, a laboratory flume test is conducted to reveal the failure process, mode, and mechanism of the loess fill slope under rainfall conditions. The variations of water contents, pore water pressure, and soil pressure are monitored in real time until the apparent failure occurred on the loess fill slope. Based on these monitoring data, the influence of weak interface on the seepage field, stress field, and deformation field of loess fill slopes triggered by rainfall are explored and analyzed, thus revealing the deformation and damage patterns and instability mechanisms of loess fill slopes induced by rainfall, which is of great significance to the prevention and accurate prediction of loess fill slope instability.

Methods

Prototype slope and model slopes

A real loess fill slope, located in Lintong County, Shaanxi province, is selected as the geological proto for experimental loess fill slope (Fig. 1). It is a gentle slope of a pure loess fill slope with a height of 24 m and a gradient of 30°, which directly deposited on nature loess slope. On-site exploration shows that the soil of fill slope belongs to

Lishi loess, with strong collapsibility and disintegrability (Zhang et al. 2013; Zhang and Liu 2010; Li et al. 2020).

The model slope was built in a 5.0 m × 1.0 m × 1.0 m (length × width × height) rigid model box. The side and bottom plates of the box are non-magnetic transparent Plexiglas plates with a thickness of 3 cm. In addition, three sets of automatic lifting and shifting devices are equipped at the front, middle, and back ends of the simulation box, which can be used to split and combine the simulation box, and can also realize the simulation of slopes with different slope angle. The simulation box is also equipped with an artificial rainfall system, high magnification camera photography, stress sensor, pore water pressure sensor, and stress–strain acquisition system. According to the experience of previous experimental studies, combined with the operability of this test, the size of this landslide physical model was determined as 1.4 m × 1.0 m × 0.3 m, the slope angle is 30° (Fig. 2); the model slope was constructed by the layered filling method during the test, and the dry density and moisture content of the loess fill slope were controlled to remain the same as the prototype slope during the filling process, with a gravity similarity constant of 1.0. By way of laboratory tests and following the standard for soil test methods (ASTM 2017), we measured the basic physical parameters of soil in the model

tests are shown in Table 1. Considering the size effect of the test model box, the loess sample was broken by hammers and passed through a 5-mm screen. The grain size distribution in Fig. 3 shows that soil particle size > 0.05 mm accounted for 4%, between 0.005 and 0.05 mm particle size accounted for 61.9%, < 0.005 mm particle size accounted for 34.1%, the test loess particles are mainly composed of powder particles.

Sensor selection and placement

The sensor instruments used in this study were comprised of four main components, including the volumetric water content sensors, pore water pressure sensors, soil pressure sensors, and data acquisition instruments (Fig. 4). The objective of this experiment was to investigate the rainfall infiltration and internal stress response characteristics of the filled loess slope. To achieve this, the volumetric water content sensor was selected to monitor the slope’s internal water infiltration characteristics, while the pore water pressure sensor and soil pressure sensor were used to observe the internal stress response characteristics. The YBY-4010 data acquisition instrument was used to perform data acquisition at a frequency of once every half minute. Figure 5 illustrates the placement of the volumetric water content,

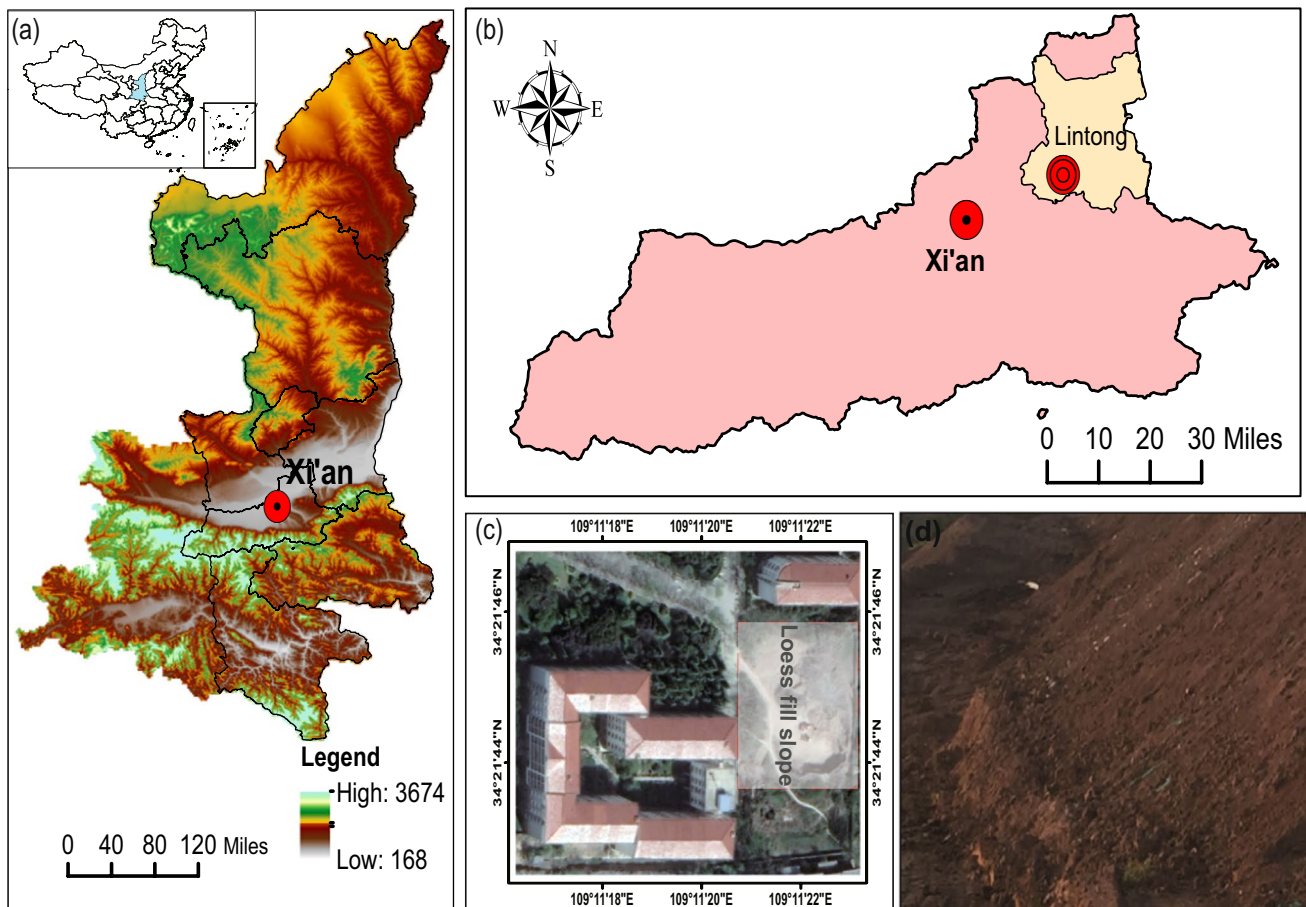


Fig. 1 The loess fill slope in Lintong County. a, b, c The location of study area; d prototype fill loess slope in the study area

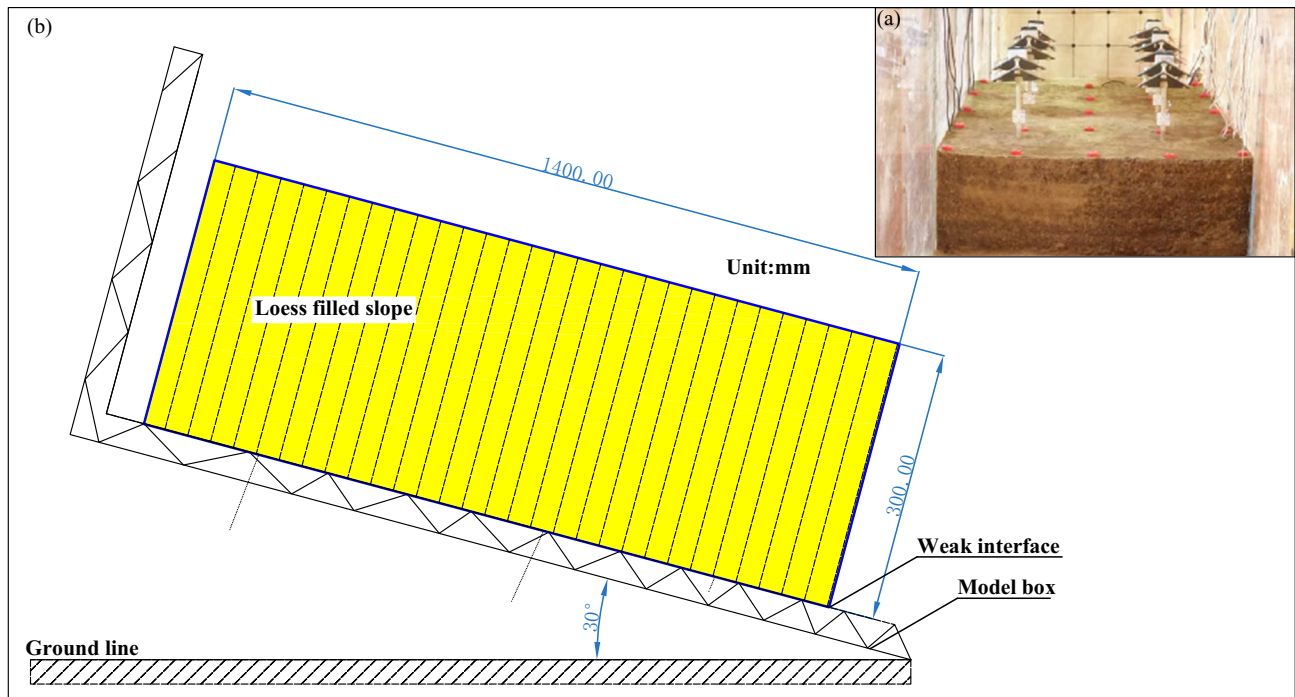


Fig. 2 Model slope and sectional dimensions (unit: mm). **a** The physical picture of model; **b** schematic diagram of the model

pore water pressure, and soil pressure sensors within the slope body. To minimize the influence of the boundary effect on the sensor monitoring results, the sensors were arranged outside the boundary effect zone. Previous studies have shown that the boundary effect range is usually 1/10 of the model width (Zhou et al. 2020; Luo et al. 2021; Zhang et al. 2021); however, in order to ensure the complete elimination of the influence of the boundary effect and the reliability of the test results, the boundary effect range in this study was determined to be 1/5 of the length of the model, equivalent to 200 mm. Three layers of sensors were placed parallel to the horizontal plane inside the slope, with the vertical distance between two adjacent layers of sensors being 100 mm. A “square grid” monitoring network was formed using three longitudinal monitoring lines and three transverse monitoring lines on each sensor plane, with the spacing between two adjacent longitudinal monitoring lines being 300 mm, and the spacing between two adjacent transverse

monitoring lines being 500 mm. Three sensors of the same type were placed on the same transverse monitoring line, resulting in a total of 9 volumetric water content sensors, 9 pore water pressure sensors, and 9 soil pressure sensors being placed in the test.

Artificial rainfall tests

The rainfall test was conducted at Xi’an University of Science and Technology’s large geological disaster physical simulation laboratory using an artificial rainfall device. The apparatus comprised a bucket, a submersible pump, flow statements, a pressure gauge, hoses, and a nozzle, with a rainfall height of 5 m (Fig. 6a). To ensure that the generated raindrops covered an area larger than the model area, the water supply pipe branch was densely arranged. The sprinkling system was calibrated before testing to arrange the spray nozzles reasonably and guarantee rainfall uniformity greater than 80% (Fig. 6b). The rainfall intensity was determined as 68 mm/h, which belongs to heavy rainfall conditions, based on the classification standard of rainfall intensity of the China Meteorological Administration and the meteorological data of Lintong County. During the test, continuous long-time rainfall was used, and the slope surface’s macroscopic deformation characteristics were monitored in real-time by a high-magnification camera. Soil pressure, volumetric water content, and pore water pressure were recorded every 30 s. The test was terminated if obvious deformation or overall landslide occurred on the slope.

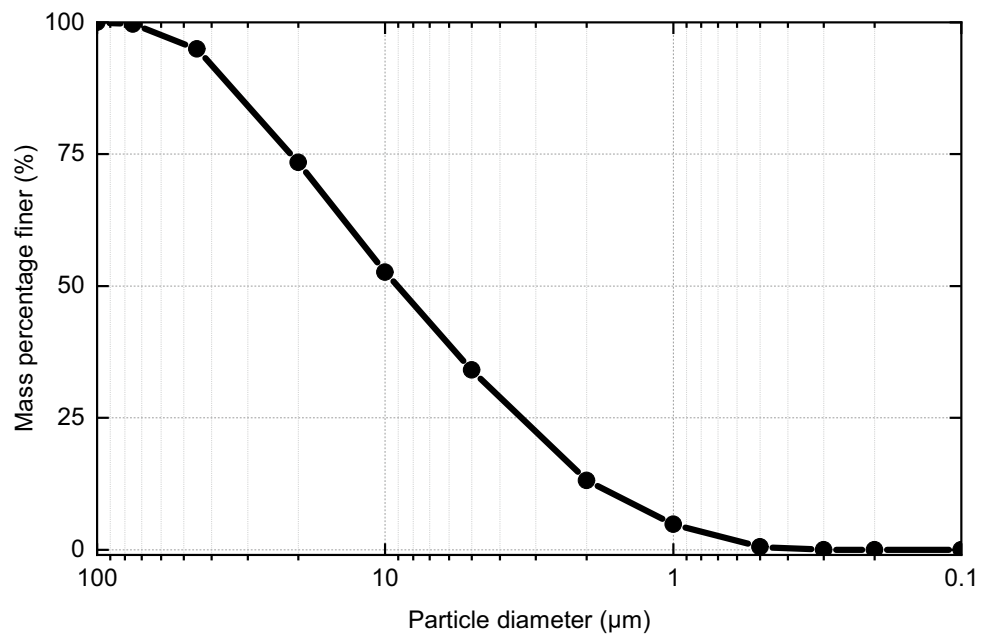
The rainfall test lasted 6025 s, and the rainfall uniformity reached 82.98% (Fig. 6c), meeting the requirement of rainfall uniformity.

Table 1 Physical properties of loess in the model tests HOA

W (%)	ρ (g/cm ³)	e	G_s	ω_p (%)	ω_L (%)
16.68	1.66	0.90	2.70	18.53	30.55
I_p	I_L	a_{1-2} (MPa ⁻¹)	E_s	c /kPa	φ (°)
11.02	-0.17	0.273	0.16	68.25	38.73

W represents water content, ρ represents natural density, e represents void ratio, G_s represents specific gravity, ω_L represents liquid limit water content, ω_p represents plastic limit water content, I_p represents plasticity index, I_L represents liquidity Index, a_{1-2} represents the coefficient of compressibility; E_s represents modulus of compressibility, c represents cohesion, φ represents internal friction angle

Fig. 3 Grain size distribution of tested loess soil



Results

Volumetric water content response of fill slope during rainfall

The variation curves of volumetric water content at the slope toe, mid-slope and slope crest are shown in Fig. 7.

Figure 7a shows that rainfall infiltration resulted in an abrupt change in the W_3 volumetric water content sensor at the foot of the slope. The W_3 volumetric water content increased from 23.73 to 39.85% in a linear trend with

increasing rainfall time. Once the soil water content reached 39.85%, the W_3 volumetric water content stabilized and remained consistent as rainfall continued to infiltrate. Further infiltration caused the W_2 volumetric water content sensor to change, with the W_2 volumetric water content increasing from 23.73 to 39.85% at an average rate of 3.5%/min. As the weight of the overburden increased, the slip force along the weak interface between the fill slope and the bedrock/natural slope increased, leading to sliding at the foot of the slope before rainwater infiltrated at W_1 . As a result, the W_1 water content sensor remained constant.

Fig. 4 Sensors instruments used in experiments. **a** Volumetric water content sensor; **b** pore water pressure sensor; **c** soil pressure sensor; **d** YBY-4010 data acquisition instrument

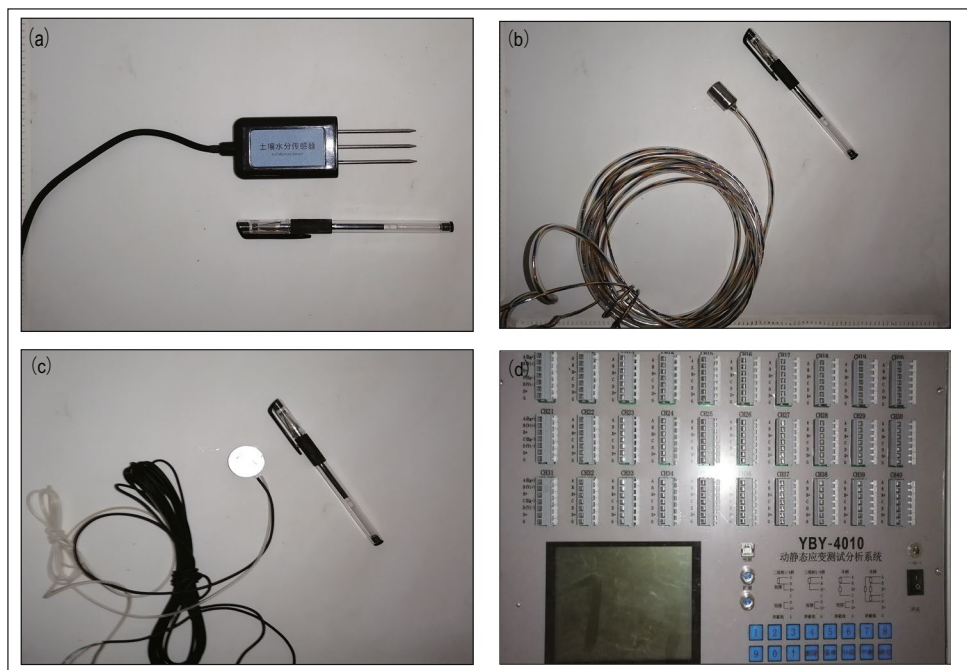
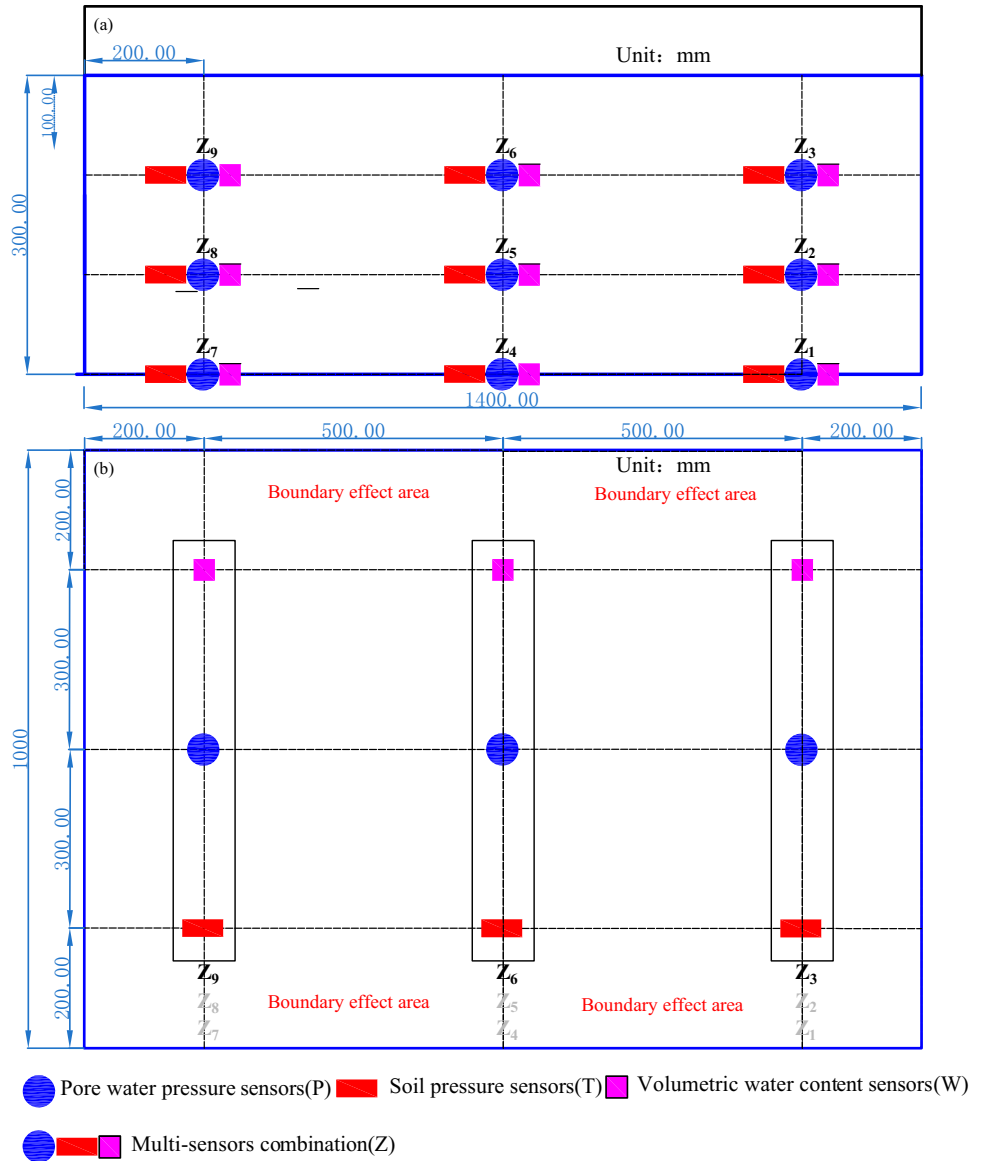


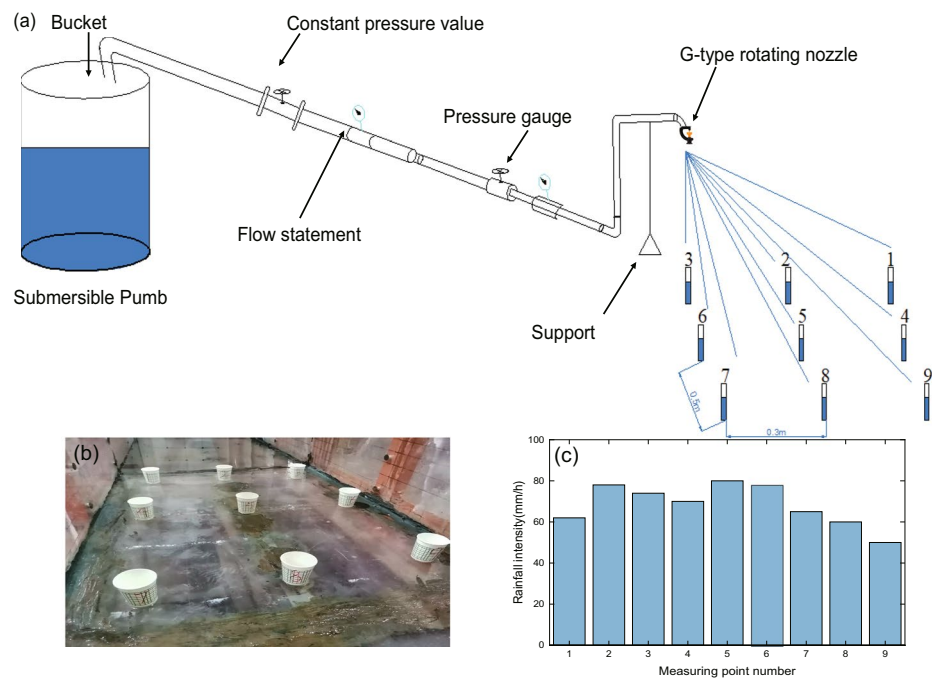
Fig. 5 Schematic design of the location of sensors. **a** Side view; **b** plane view



As can be seen from Fig. 7b, the initial change in W_4 volumetric water content sensor occurred due to tilted horizontal infiltration along the weak interface. This caused the volumetric water content to increase from 23.73 to 37.45% with an average rate of 0.81%/min at mid-slope. Once the volumetric water content of W_4 became stable, the vertical infiltration of rainfall led to a change in the W_6 sensor. The volumetric water content increased from 23.73 to 38.65%, with an average rate of increase of 0.38%/min. The combined effect of inclined horizontal infiltration and vertical infiltration resulted in an increase in W_5 volumetric water content from 23.73 to 40.89%. The average rate of increase of water content in W_5 was much higher than that of W_4 and W_6 volumetric water content sensors, at 2.29%/min.

As shown in Fig. 7c, the volumetric water content of W_7 , W_8 , and W_9 all exhibited a three-stage trend of “uniform increase—slow increase—stable constant” as the duration of rainfall increased. However, the horizontal infiltration along the weak interface inclined caused the W_7 and W_8 volumetric water content sensors to change earlier at the top of the slope, saturating the contact soil with water and reducing the shear strength. After the W_7 and W_8 volumetric water content sensors essentially remained unchanged, the W_9 volumetric water content gradually increased. This led to an increase in the weight of the overlying soil, further reducing the slip resistance, increasing the slip forces, and ultimately resulting in a misaligned collapse of the soil at the top of the slope.

Fig. 6 The layout of the Artificial rainfall tests showing. **a** Test equipment; **b** calibration tests for rainfall spray nozzles; **c** results of calibration tests



Soil pressure response of fill slope during rainfall

The variation curves of soil pressure at the slope toe, mid-slope, and slope crest are shown in Fig. 8.

Figure 8a illustrates the three-stage trend of the soil pressure of T_1 and T_2 , which can be described as “stable and gentle—gradually increasing—gradually decreasing.” The infiltration of rainwater leads to saturation of the soil with water and increases its self-weight, resulting in a gradual increase in the soil pressure of T_1 and T_2 . This soil pressure reaches a peak value at approximately 3270 s. Subsequently, the slope toe enters the microfracture development stage, and as the microfracture progresses and expands, the internal stress of the soil is unloaded, leading to a gradual decrease in the soil pressure until the slope toe eventually slides. Moreover, it was observed that the T_3 soil pressure data decreased sharply when the rainfall duration was approximately 2000s. This phenomenon was attributed to the local disintegration of the soil at the top of the slope toe, which led to a decrease in the thickness of the soil. Overall, these findings provide valuable insights into the dynamic behavior of soil pressure in relation to rainfall-induced landslides.

As can be seen from Fig. 8b, the inclined infiltration along the weak interface initially resulted in changes in the T_4 soil pressure sensor. As the inclined infiltration intensified, the self-weight of the soil increased, causing gradual increases in both the T_4 and T_5 soil pressures, with a peak observed at around 4140 and 2500 s, respectively. At this stage, the T_6 soil pressure sensor showed no significant changes due to the low vertical infiltration of the topsoil and

the small thickness of the soil layer. Approximately 4000 s later, continuous infiltration of rainfall caused spalling and migration of soil particles within the soil body, leading to the development of microfractures at mid-slope. This resulted in a gradual decrease in soil pressure until local sliding occurred at mid-slope.

According to the findings presented in Fig. 8c, it can be observed that the inclined infiltration along the weak interface leads to an increase in the soil weight at the bottom, with the T_7 soil pressure sensor being the first to increase until the bottom soil is fully saturated by around 1000 s of rainfall. However, as the rainfall continued, the vertical infiltration of the rainfall led to an increase in the weight of the overlying soil layer, and the T_7 , T_8 , and T_9 soil pressure sensors grew simultaneously at around 3000 s, before the soil pressure remained relatively stable at around 4000 s. As the rainfall continues, we find that the T_7 soil pressure sensor decreases first, due to the development of microfractures in the soil at the bottom caused by the sloping infiltration of the weak interface. With the development of microfractures at the bottom, the soil shear strength further decreases and the slope slides along the weak interface in an overall misaligned sliding pattern, resulting in an instantaneous decrease in T_7 , T_8 , and T_9 soil pressure sensors.

Pore water pressure response of the fill slope during rainfall

The variation curves of pore water pressure at the slope toe, mid-slope, and slope crest are shown in Fig. 9.

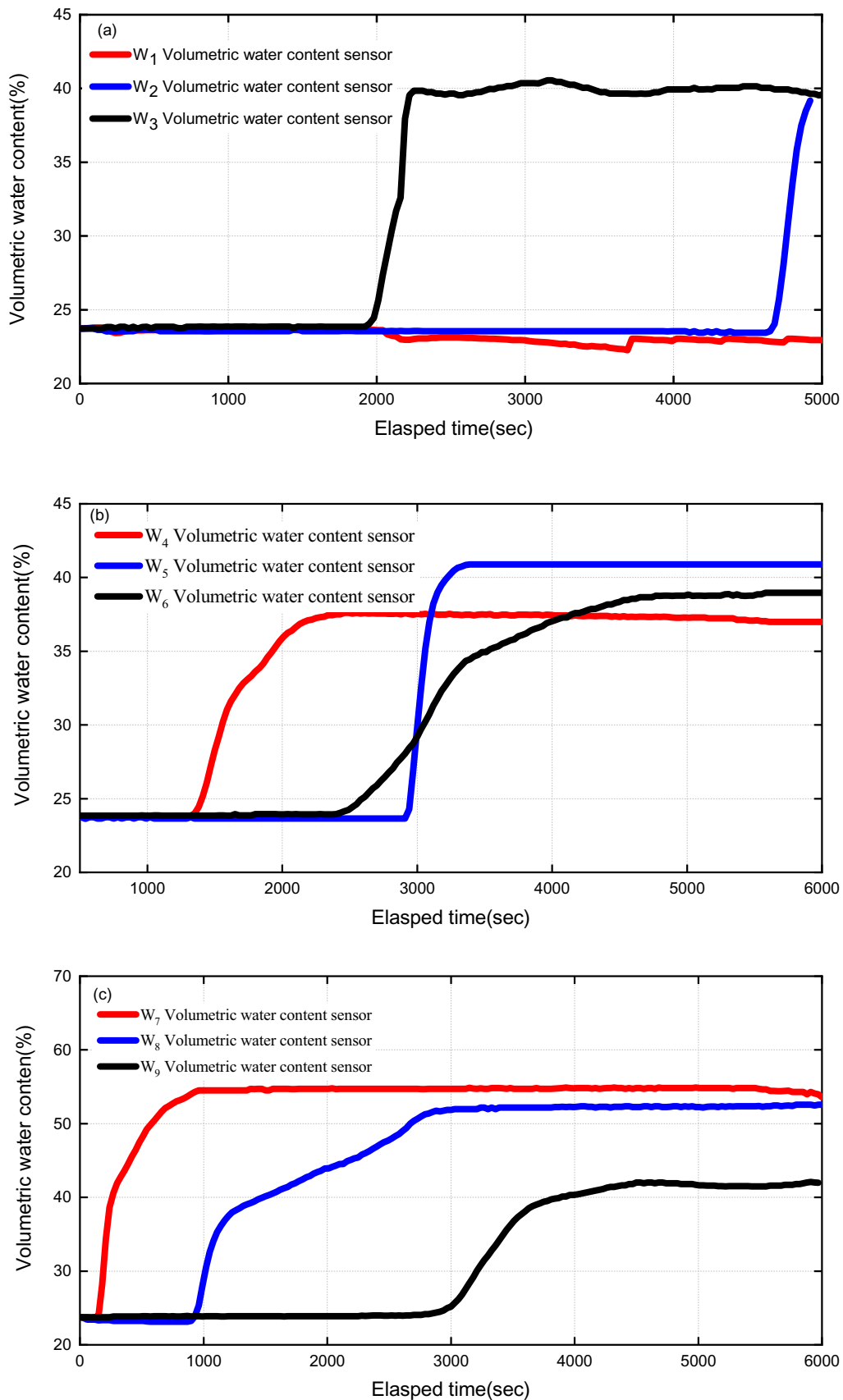
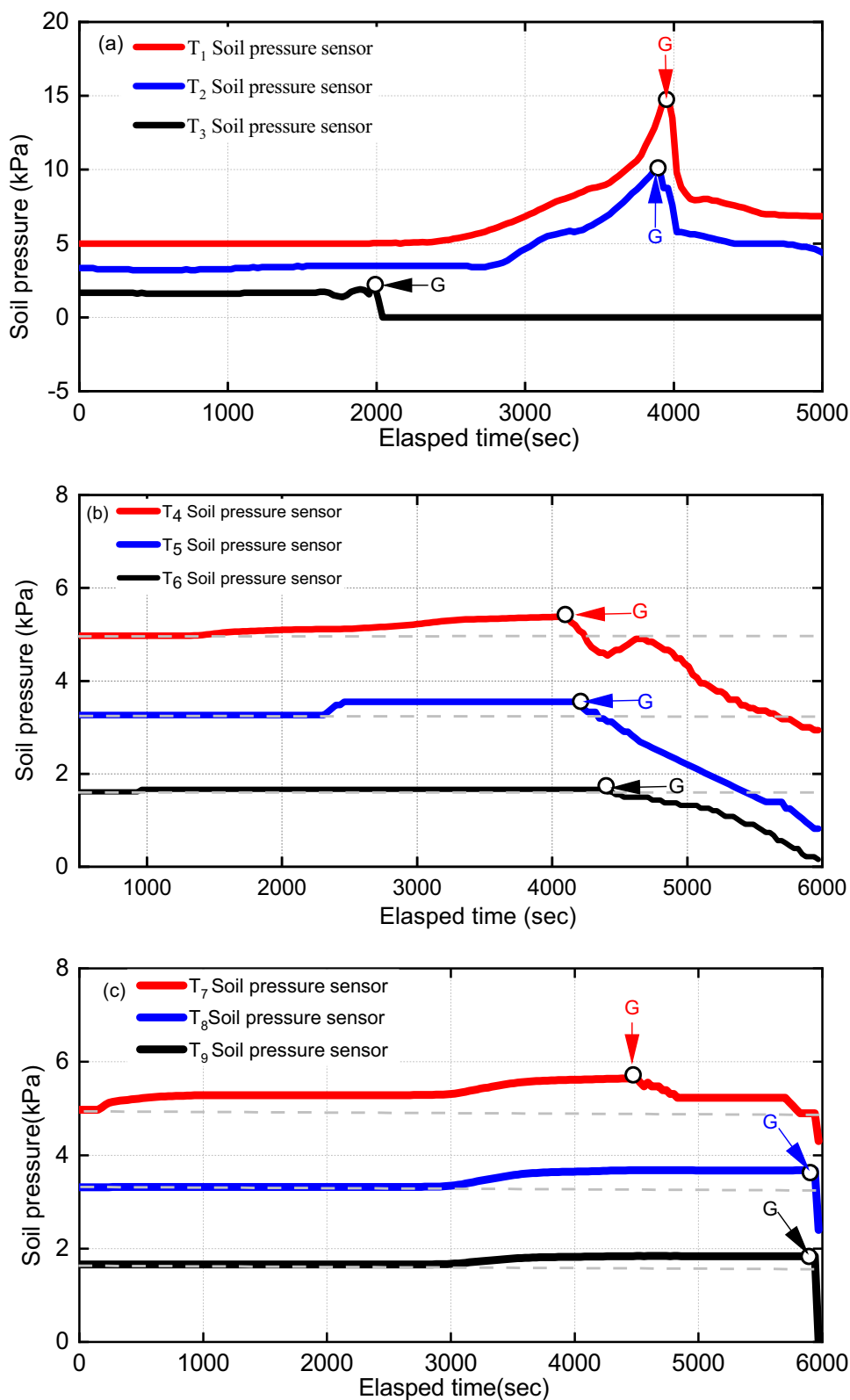


Fig. 7 The variation curves of volumetric water content with time under rainfall conditions. **a** slope toe; **b** mid-slope; **c** slope crest

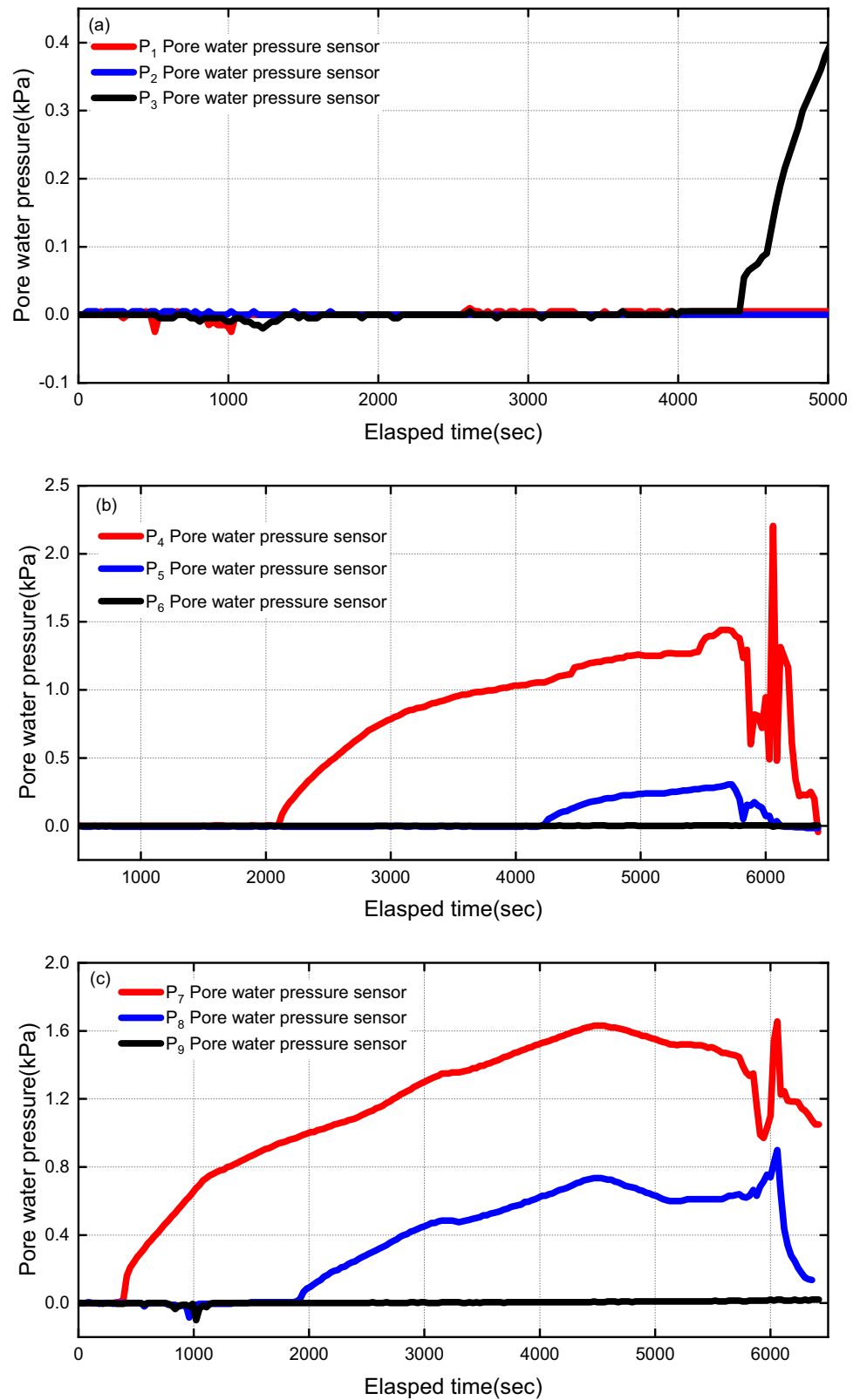
Fig. 8 The variation curves of soil pressure with time under rainfall conditions. **a** Slope toe; **b** mid-slope; **c** slope top. *G* represents starting point for soil pressure reduction



As shown in Fig. 9a, the pore water pressure values at P₁ and P₂ located at the slope toe remain constant at 0 throughout the rainfall duration. Conversely, when the duration of

rainfall reached 4410 s, the pore water pressure value at P₃ began to increase linearly. Once the pore water pressure value reached 0.4 kPa, the soil at the slope toe collapsed.

Fig. 9 The variation curves of pore water pressure with time under rainfall conditions. **a** Slope toe; **b** mid-slope; **c** slope crest



The volumetric water content sensor W_1 remained almost unchanged during the entire duration of the experiment, indicating that there was no water infiltration at this particular

location. Therefore, the corresponding pore water pressure value for P_1 was consistently 0. When the test results of volumetric water content for W_2 and W_3 were combined with

the pore water pressure data for P_2 and P_3 , it was observed that there was significant hysteresis in the response time of pore water pressure inside the fill slope caused by rainfall conditions when compared to the response time of volumetric water content. This was attributed to the fact that the volumetric water content changes immediately once the wetting front reaches the sensors, while the pore water pressure changes only after the infiltration water passes through the permeable stone of the pore water pressure sensors.

Figure 9b reveals the behavior of pore water pressure at various depths along the mid-slope. Pore water pressure readings from the P_6 sensor located at a buried depth of 100 mm were consistently 0 and unchanged throughout the rainfall duration. However, readings from the P_4 and P_5 sensors showed a change at rainfall durations of 2100s and 4200 s, respectively. The pore water pressure gradually increased with increasing rainfall duration. At a rainfall duration of 5700 s, the pore water pressure values for P_4 and P_5 began to decrease, with P_5 showing a continuous decreasing trend and P_4 exhibiting fluctuating decreases. The maximum values of pore water pressure observed during the rainfall were 2.2 kPa for P_4 and 0.3 kPa for P_5 .

Figure 9c reveals the pore water pressure trends at various depths along the slope top. Sensor P_9 , located at a buried depth of 100 mm, showed a consistent and unchanged pore water pressure reading of 0 throughout the rainfall duration. Pore water pressure changes in P_7 and P_8 sensors were similar, exhibiting a four-stage change trend of “slowly increasing—gradually decreasing—sharply increasing—sharply decreasing.” The pore water pressure at P_7 and P_8 sensors changed at rainfall durations of 300 s and 1860s, respectively, showing a gradual increase in values. As the rainfall duration reached 4500 s, the pore water pressure of P_7 and P_8 sensors gradually decreased with readings of 0.99 kPa and 0.6 kPa, respectively. The pore water pressure of P_7 and P_8 sensors then gradually increased, growing to a maximum of 1.66 kPa and 0.9 kPa, respectively. After reaching maximum values, the pore water pressure of P_7 and P_8 sensors sharply decreased, and the slope ultimately failed.

Discussion

Seepage characteristics analysis of loess fill slope induced by rainfall

Due to slope damage tends to occur when the volumetric water content is at maximum value, and the volumetric water content responds to rainfall earlier than the pore water pressure (Abramson et al. 1996; Eichenberger et al. 2013), in-depth analysis of rainfall seepage characteristics within the slopes of loess fills becomes the key to analyzing slope failure patterns and failure mechanisms (Hakro and Harahap

2015; Fan and Wang 2019). Assuming that rainfall infiltrates perpendicular to the face of the fill and along the weak interface between the fill and the bedrock/natural slope, the initial growth response time of the volumetric water content can be analyzed to reveal the predominant form of infiltration on the fill slope (Fig. 10a). Figure 10b shows that the initial growth response time of the sensors on the weak interface (W_7, W_4) is much earlier than that of the other water content sensors inside the fill slope ($W_9, W_8, W_6, W_5, W_3, W_2$), indicating a predominance of tilted infiltration at the base of the fill slope. Comparing the results of the volumetric water content sensor tests at burial depths of 10 cm and 20 cm respectively, the initial growth response times of the W_8 and W_5 volumetric water content sensors are 15 min and 41 min, which are earlier than the initial growth response times of the upper volumetric water content sensors (W_9 and W_6) of 48 min and 48.5 min, while the initial growth time of the W_2 volumetric water content sensor is 77.5 min, which is, later than the upper volumetric water content sensor (W_3) and the same depth of burial sensor (W_5), implying that tilted infiltration occurs mainly at W_8 and W_5 volumetric water content sensors and coupled vertical and tilted infiltration of rainfall may occur at W_2 volumetric water content sensor. Based on the migration modes, migration distance and migration time, the migration rate of wetting front can be calculated, as shown in Table 2. The data show that the maximum migration rate of the wetting front perpendicular to the fill loess slope is 13.3×10^{-3} m/min, and the maximum migration rate of the wetting front along the weak interface is about 71×10^{-3} m/min, which is about five times higher than in loess fill. In addition, we found that at the same depth of burial, the volumetric water content sensors (W_9, W_6, W_3) migrated at a rate of 2.4×10^{-3} m/min, 2.5×10^{-3} m/min, and 13.3×10^{-3} m/min respectively, with the maximum vertical migration rate at slope toe surface (Fig. 10c). This is because the slope angle of the loess fill slope is 30° , part of the upper rainwater on the slope surface perpendicular to the slope surface occurs vertical infiltration, and the other part occurs runoff along the slope surface, resulting in increasing migration rate of the wetting front at slope toe surface.

In this paper, the migration characteristics of the wetting fronts during the test were investigated by recording the position of the infiltration at different times on the glass on both sides of the model box and the initial response time of the volumetric water content. As shown in Fig. 13, the migration process of the wetting front can be divided into three stages: (1) partial infiltration stage (0–32 min) (2) the wetted front connection stage (32–77.5 min), and (3) the infiltration phase at the base of slope toe (77.5–100.4 min).

At the partial infiltration phase (0–32 min), the weak interface becomes the dominant path for rainfall to infiltrate into the slope, with wetting fronts appearing first at the base of the slope crest and migrating along the weak interface

Fig. 10 Seepage characteristics of loess fill slope. **a** The diagram of rainfall seepage from loess fill slope; **b** the time of began to increase with different volumetric water content sensors; **c** the migration rate with different volumetric water content sensors

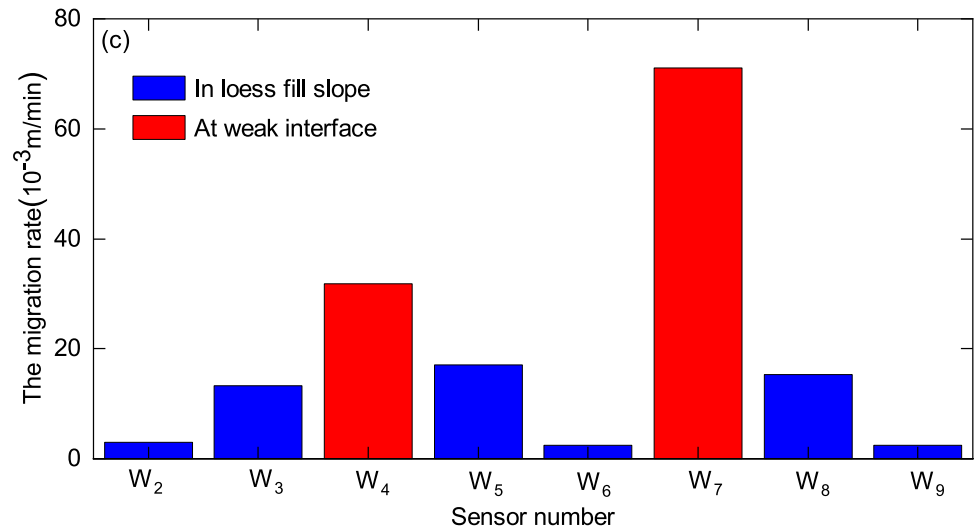
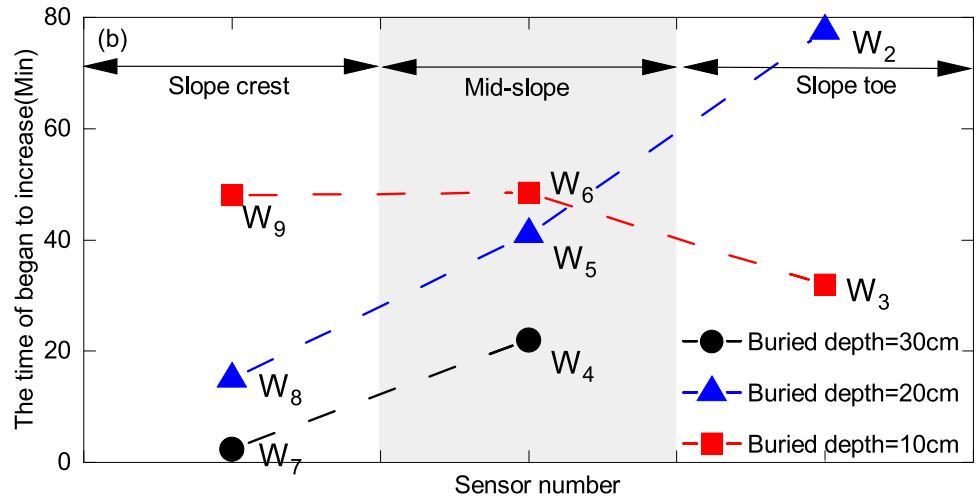
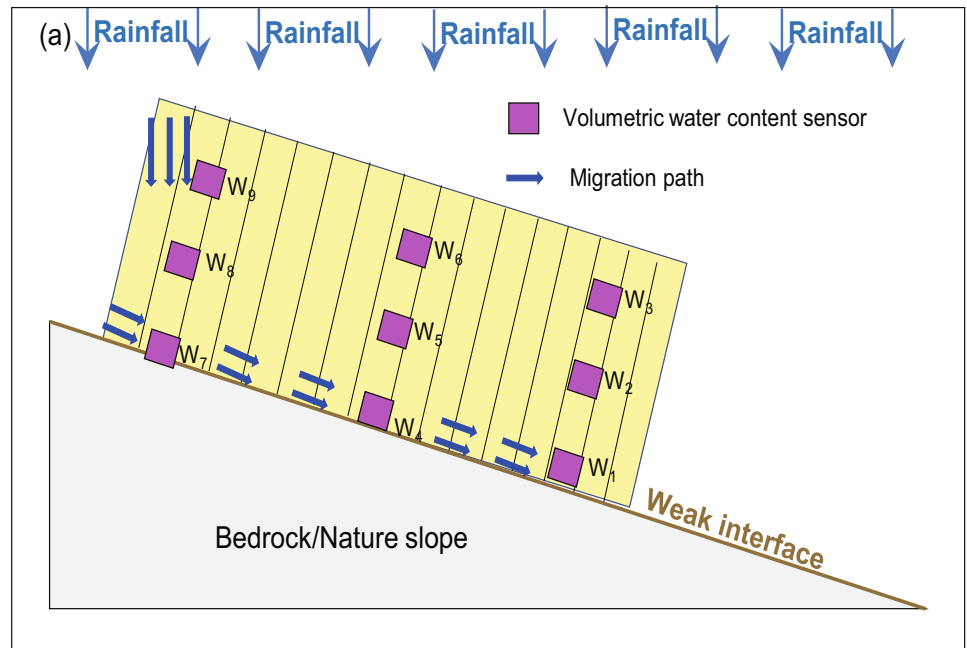


Table 2 Migration rate of wetting front

Location	In loess fill slope						At weak interface		
	W ₉	W ₆	W ₃	W ₈	W ₅	W ₂	W ₇	W ₄	W ₁
Sensors number									
Migration distances (m)	0.12	0.12	0.12	0.2	0.7	0.23	0.2	0.7	0.9
Migration time (min)	48.5	48	32	15	41	77.5	2.5	22	-
The migration rate (10 ⁻³ m/min)	2.4	2.5	13.3	15.3	17.0	3.0	71	31.8	-

towards slope toe as rainfall infiltrating (Fig. 11a). When the rainfall duration reached 32 min, vertical infiltration of rainfall causes wetting fronts to appear at the top of the foot of the slope (Fig. 11b). At the wetting front connection stage (32–77.5 min), the wetting fronts formed by vertical infiltration of rainfall gradually migrate from the slope toe to the crest, and the wetting fronts formed by tilted infiltration of the weak interface migrate from the slope crest to slope toe, and the wetting fronts are interconnected (Fig. 11c). During the infiltration phase at the base of slope toe (77.5–100.4 min), the two wetting fronts gradually expand, connect, and surround the base of the slope toe, resulting in no rainfall response at the base of the slope toe until the slope is failure (Fig. 11d). The seepage characteristics of the loess fill slope indicate that the weak interface between the fill slope and the natural slope can influence the migration of the wetting fronts by forming a preferential flow path and control the change of the seepage field of the fill loess slope, accelerating the saturation process of the fill slope.

Failure mode analysis of loess fill slope induced by rainfall

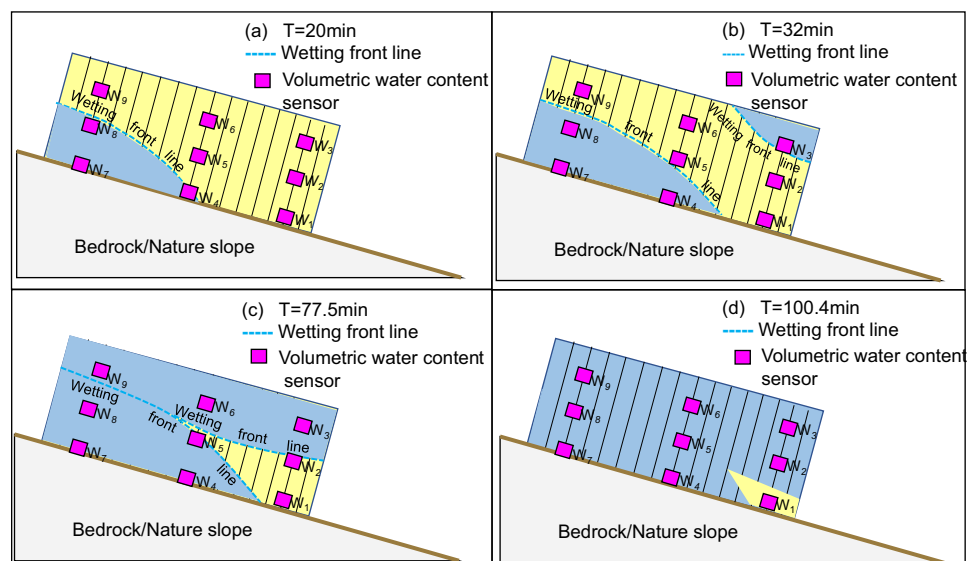
The failure mode of fill loess slopes under rainfall is closely related to various factors, including stratigraphic structure, slope morphology, seepage characteristics, and soil

properties (Chen et al. 2018; Sun et al. 2021). By combining the deformation characteristics, seepage characteristics, and stress response characteristics observed in this model test, the instability pattern of the loess fill slopes can be generalized into four stages: slope toe damage, crack development and penetration, local sliding, and overall misaligned sliding.

Slope toe damage stage: At the beginning of the rainfall, a head difference is created between the top and foot of the slope due to the slope angle and surface runoff. The runoff and infiltration of rainfall cause severe erosion to the soil at the foot of the slope. Volumetric water content sensors installed on the slope confirm that the soil at the foot of the slope (W₃) becomes saturated first, followed by the mid-slope (W₆) and top of the slope (W₉), and when rainfall duration reaches 2042s, the soil at the foot of the slope collapses, leading to a sharp drop in T₃ soil pressure (Fig. 8a).

1. Crack development and penetration stage: Subsequent to the destruction of the slope toe, the geometry, seepage, and stress conditions of the slope are altered due to the loss of support. The impact of raindrops on the loess structure of the slope creates a thin compacted layer that acts as a sealing layer on the soil surface, which further increases slope runoff and enhances erosion (Helalia et al. 1988; Moore and Singer 1990). As rainfall continues, rainwater infiltrates along the weak interface towards the slope toe, ultimately

Fig. 11 Migration process of the wetting front at different time. **a** T=20 min; **b** T=32 min; **c** T=77.5 min; **d** T=100.4 min



softening the soil and reducing its strength. This, combined with the erosion on the slope surface, creates tension cracks on the left side of the slope toe and mid-slope that gradually develop, expand, and penetrate downwards. As the cracks grow, the internal stress balance of the slope is disrupted and the soil pressure in the central part of the slope is gradually reduced (Fig. 8b). Based on the onset of soil pressure decay, it is apparent that $T_4 < T_5 < T_6$, indicating that tensile cracks are gradually penetrating upwards from the bottom.

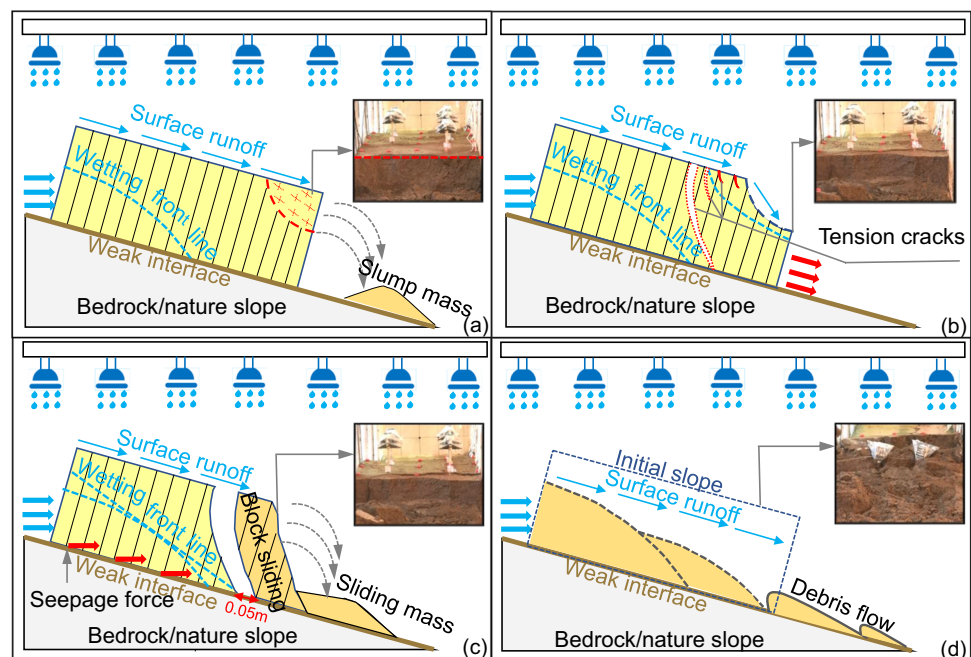
2. Local sliding stage: The presence of tensile cracks in the fill loess slope facilitates the infiltration of rainwater, which enhances the impact of rainfall on the slope. As rainfall infiltrates the slope, a transition zone is created at the base of the slope where the soil approaches saturation and the shear strength of the weak interface deteriorates. Furthermore, our observations indicate that infiltration forces and head differences are formed in the rainwater present within the cracks and at a certain depth of the slope. Due to the influence of self-weight and infiltration forces, local sliding damage occurs along the weak interface, as depicted in Fig. 12c. These findings emphasize the combined effects of rainfall infiltration, slope runoff, and the presence of tensile cracks in promoting slope instability and the development of sliding damage.
3. The overall misaligned sliding stage: After local damage occurs, the slope's geometry, seepage, and stress conditions change once again. Prolonged rainfall, however, creates preferential channels on the weak interface, leading to faster saturation of the fill slope and a subsequent deterioration of soil mechanical parameters. Additionally, these preferential channels generate seepage forces

that act on the outside of the slope, further altering the seepage and stress fields of the slope. This weakens the bond between the fill slope and the original slope, making the fill slope more vulnerable to overall misplaced sliding along the weak interface (Fig. 12d).

Failure mechanism analysis of loess fill slope induced by rainfall

Previous studies have shown that loess fill slopes are engineered slopes consisting of natural bedrock slopes, loess fill, and interfaces, making the failure mechanism of these slopes more complex than that of uniform loess slopes (Chang et al. 2021). The unique inclined geological structure of these slopes alters the internal stress distribution in the soil during rainfall, further complicating slope failure mechanisms. For instance, Wu et al. (2018) suggested that the slope is more likely to fail along the soil–bedrock contact than along the wetting front when preferential flow reaches the bedrock surface. Gerscovich et al. (2006) proposed that the preferential flow of rainfall along highly weathered bedrock at the slope crest causes a rapid rise of pore water pressure, eventually leading to slope failure. Wen et al. (2005) and Zhang et al. (2019a, b, c) similarly found that a preferential flow path formed at the interface between soil and bedrock is crucial in the hydrological processes that lead to slope failure. In conclusion, the above analysis indicates that the weak interface between the bedrock/natural slope and the fill slope plays a crucial role in determining the stability of the fill slope. Indeed, this experimental study finds that the weak interface becomes the dominant flow path under rainfall, with the wetting front progressively moving along the contact towards

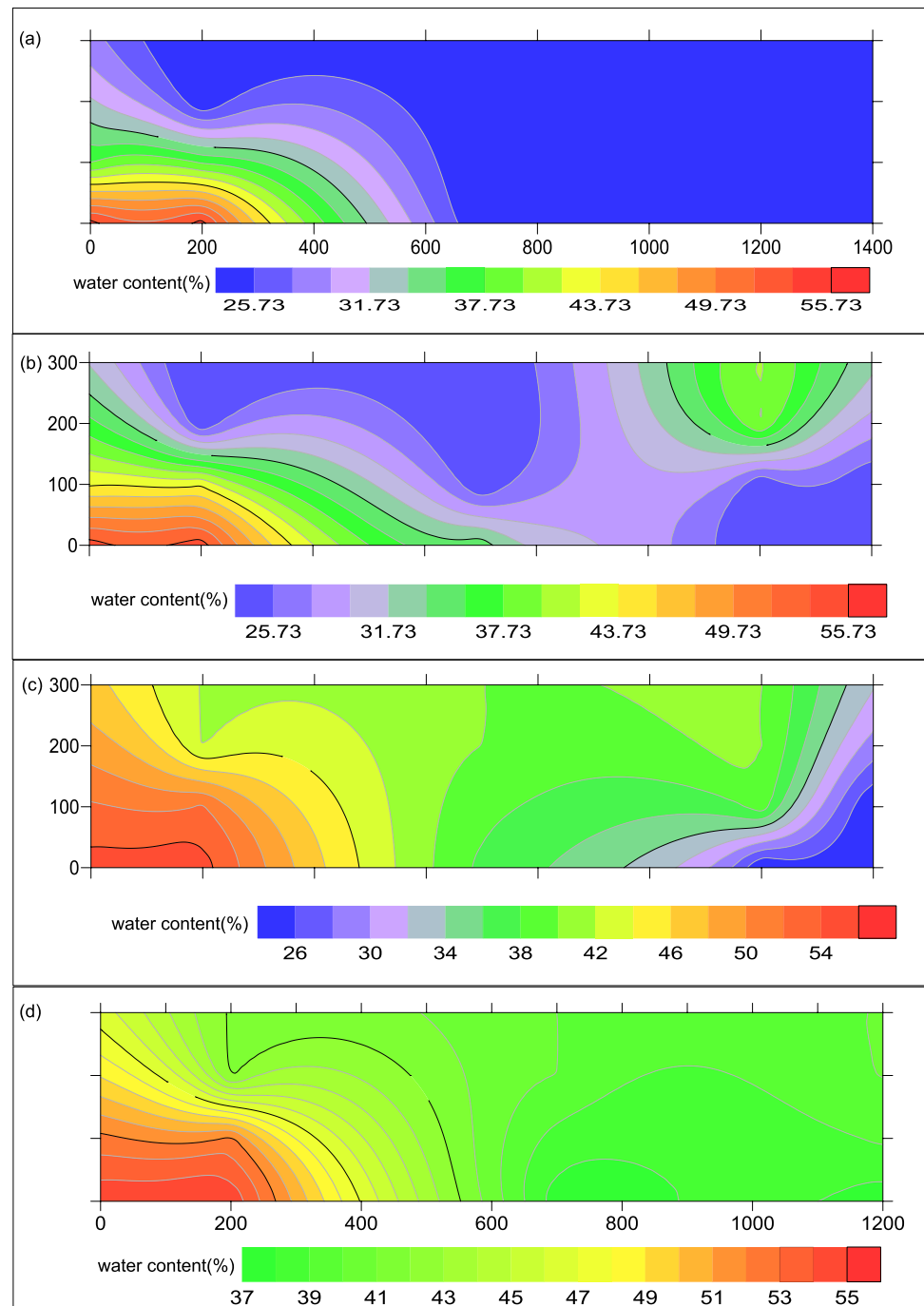
Fig. 12 Failure evolution of fill loess slope under rainfall conditions. **a** Slope toe damage stage; **b** crack development and penetration stage; **c** local sliding stage; **d** the overall misaligned sliding stage



the foot of the slope, and the soil at the weak interface becoming saturated first (Fig. 11). From the moisture content contour plot, it can be seen that during rainfall, the weak interface soil has a higher volumetric moisture content, the maximum pore water pressure, reduced shear strength, and reduced slip resistance of the weak interface (Fig. 13). In addition, vertical infiltration into the slope as well as surface runoff cause damage to the toe of the slope, the slope loses support, and local sliding of the soil occurs along the weak interface. After local sliding of the slope, the slope loses support at the trailing edge and the

stress conditions changed in the slope. The continuous rainfall inclined seepage action causes seepage forces to be generated outwards on the weak interface and the slip resistance of the soil on the weak interface is reduced. Under the influence of multiple factors of self-weight and infiltration, the sliding force of the loess fill slope increases, the slip resistance decreases, and the slope body undergoes overall misaligned sliding. The test results show that the weak interface between the bedrock/natural slope and the loess fill slope becomes the dominant channel for rainwater infiltration into the slope, and there is

Fig. 13 Volumetric water content contour map. **a** $T=20$ min; **b** $T=32$ min; **c** $T=77.5$ min; **d** $T=100.4$ min



relatively high pore water pressure on the weak interface, which makes the fill slope more prone to trigger landslides along the weak interface, and the failure mode is slip-tensioning. Therefore, the preferential flow path formed on the weak interface should always be considered in the engineering control of the fill slope (Guo et al. 2023). In summary, it can be seen that the weak interface of the fill slope controls the failure mechanism of the slope. On the one hand, the existence of the weak interface makes the slope inclined infiltration rate greater than the vertical infiltration rate, and the weak interface becomes the dominant channel for rainfall infiltration, with the largest pore water pressure and the lowest strength of the soil on the weak interface. On the other hand, its special geologic structure provides sliding surfaces for the occurrence of the fill landslides, which accelerates the destabilizing damage of the slope. Therefore, the weak interface of fill slopes becomes a non-negligible factor in analyzing the failure mechanism of fill slopes.

Conclusions

This study presents an experimental investigation of the hydrological characteristics, damage modes, and damage mechanisms of rainfall-induced loess slopes through flume tests, elucidating the failure evolution of the slope, stress response characteristics, and the impact of the weak interface on slope failure under rainfall conditions. The research findings have important implications for the prevention and management of slope instability and disaster prediction of loess fill slopes. The following are the key conclusions of our study:

1. During rainfall duration, vertical infiltration and tilted infiltration along the weak interface occurred in loess fill slope. The maximum migration rate of the wetting front perpendicular to the slope surface is 13.3×10^{-3} m/min, and the maximum migration rate of the wetting front along the weak interface is 71×10^{-3} m/min, which is about five times that of the vertical wetting front rate. This indicates that the weak interface between the fill slope and the bedrock/natural slope becomes the dominant flow path for rainfall infiltration and controls the change of seepage field of the fill loess slope, accelerating the saturation process of the fill slope.
2. The dominant flow path along the weak interface between the original slope and the fill slope not only accelerates the saturation of the slope and leads to deterioration of the mechanical properties of the soil, but also generates permeability towards the outside of the slope, thus changing the seepage and stress field of the fill slope, weakening the adhesion between the fill slope and the bedrock, with the maximum pore water pressure on the weak interface and making the fill slope more susceptible to sliding along the weak interface.
3. According to the variation characteristics of the volume water content, pore water pressure and horizontal soil pressure of the loess fill slope, combined with the slope deformation, the failure mode of the loess fill slope induced by rainfall belongs to the slip-tensioning type, which shows the gradual failure from the slope toe to slope crest. At the beginning of the rainfall, local failure occurs at the slope toe and the slope loses its support. As the rainfall continues, the slope slides along the weak interface at multiple levels, triggering traction landslides.

Funding This study was partially funded by the Strategic Priority Research Program of the Chinese Academy of Sciences (grant no. XDA23090202) and the National Natural Science Foundation of China (grant nos. U20A20112 and 41790432). Yao Jiang acknowledges support from the CAS Pioneer Hundred Talents Program. A special acknowledgment should be expressed to China–Pakistan Joint Research Center on Earth Sciences that supported the implementation of this study.

Declarations

Competing interests The authors declare no competing interests.

References

- Abramson L, Lee T, Sharma S, Boyce G (1996) Slope stability and stabilization methods. Wiley, New York, p 629
- Askarinejad A, Akca D, Springman SM (2018) Precursors of instability in a natural slope due to rainfall: a full-scale experiment. *Landslides* 15:1745–1759. <https://doi.org/10.1007/s10346-018-0994-0>
- ASTM (2017) Standard practice for classification of soils for engineering purposes (unified soil classification system). ASTM standard D2487- 17. West Conshohocken, Pennsylvania: American Society for Testing Materials
- Bentley MJ, Foster JM, Potvin JJ, Bevan G, Sharp J, Woeller DJ, Take WA (2023) Surface displacement expression of progressive failure in a sensitive clay landslide observed with long-term UAV monitoring. *Landslides* 20:531–546. <https://doi.org/10.1007/s10346-022-01995-4>
- Chang Z, Huang F, Huang J, Jiang S-H, Zhou C, Zhu L (2021) Experimental study of the failure mode and mechanism of loess fill slopes induced by rainfall. *Eng Geol* 280. <https://doi.org/10.1016/j.enggeo.2020.105941>
- Chen G, Meng X, Qiao L, Zhang Y, Wang S (2018) Response of a loess landslide to rainfall: observations from a field artificial rainfall experiment in Bailong river basin, China. *Landslides* 15:895–911. <https://doi.org/10.1007/s10346-017-0924-6>
- Chen WW, Zhang S (2021) Gis-based comparative study of Bayes network, Hoeffding tree and logistic model tree for landslide susceptibility modeling. *Catena* 203. <https://doi.org/10.1016/j.catena.2021.105344>
- Chen Y, Li B, Xu Y, Zhao Y, Xu J (2019) Field study on the soil water characteristics of shallow layers on red clay slopes and its application in stability analysis. *Arab J Sci Eng* 44:5107–5116. <https://doi.org/10.1007/s13369-018-03716-3>
- Cho SE (2016) Stability analysis of unsaturated soil slopes considering water-air flow caused by rainfall infiltration. *Eng Geol* 211:184–197. <https://doi.org/10.1016/j.enggeo.2016.07.008>

- Cui P, Guo CX, Zhou JW, Hao MH, Xu FG (2014) The mechanisms behind shallow failures in slopes comprised of landslide deposits. *Eng Geol* 180:34–44. <https://doi.org/10.1016/j.enggeo.2014.04.009>
- Deng L, Fan W, Yu M (2018) Parametric study of a loess slope based on unified strength theory. *Eng Geol* 233:98–110. <https://doi.org/10.1016/j.enggeo.2017.11.009>
- Eichenberger J, Ferrari A, Laloui L (2013) Early warning thresholds for partially saturated slopes in volcanic ashes. *Comput Geotech* 49:79–89. <https://doi.org/10.1016/j.compgeo.2012.11.002>
- Elkamhawey E, Wang HB, Zhou B, Yang ZY (2018) Failure mechanism of a slope with a thin soft band triggered by intensive rainfall. *Environ Earth Sci* 77. <https://doi.org/10.1007/s12665-018-7538-8>
- Fan CC, Wang HZ (2019) The behavior of wetting front on slopes with different slope morphologies during rainfall. *J Hydro-Environ Res* 25:48–60. <https://doi.org/10.1016/j.jher.2019.07.005>
- Gerscovich DMS, Vargas EA, de Campos TMP (2006) On the evaluation of unsaturated flow in a natural slope in Rio de Janeiro. *Brazil Eng Geol* 88:23–40. <https://doi.org/10.1016/j.enggeo.2006.07.008>
- Guo Z, Huang Q, Liu Y, Wang Q, Chen Y (2023) Model experimental study on the failure mechanisms of a loess-bedrock fill slope induced by rainfall. *Eng Geol* 313:106979. <https://doi.org/10.1016/j.enggeo.2022.106979>
- Hakro MR, Harahap ISH (2015) Laboratory experiments on rainfall-induced flowslide from pore pressure and moisture content measurements. *Nat Hazards Earth Syst Sci Discuss* 2015:1575–1613. <https://doi.org/10.5194/nhessd-3-1575-2015>
- He SQ, Qin F, Zheng ZC, Li TX (2018) Changes of soil microrelief and its effect on soil erosion under different rainfall patterns in a laboratory experiment. *CATENA* 162:203–215. <https://doi.org/10.1016/j.catena.2017.11.010>
- Helalia AM, Letey J, Graham RC (1988) Crust formation and clay migration effects on infiltration-rate. *Soil Sci Soc Am J* 52:251–255. <https://doi.org/10.2136/sssaj1988.03615995005200010044x>
- Lee LM, Gofar N, Rahardjo H (2009) A simple model for preliminary evaluation of rainfall-induced slope instability. *Eng Geol* 108:272–285. <https://doi.org/10.1016/j.enggeo.2009.06.011>
- Li YR, Shi WH, Aydin A, Beroya-Eitner MA, Gao GH (2020) Loess genesis and worldwide distribution. *Earth Sci Rev* 201. <https://doi.org/10.1016/j.earscirev.2019.102947>
- Lim TT, Rahardjo H, Chang MF, Fredlund DG (1996) Effect of rainfall on matrix suction in a residual soil slope. *Can Geotech J* 33:618–628. <https://doi.org/10.1139/t96-087>
- Luca F, D'Ambrosio D, Robustelli G, Rongo R, Spataro W (2014) Integrating geomorphology, statistic and numerical simulations for landslide invasion hazard scenarios mapping: an example in the Sorrento peninsula (Italy). *Comput Geosci* 67:163–172. <https://doi.org/10.1016/j.cageo.2014.01.006>
- Luo Y, Zhang JM, Zhou Z, Shen ZJ, Chong L, Victor C (2021) Investigation and prediction of water infiltration process in cracked soils based on a full-scale model test. *Geoderma* 400. <https://doi.org/10.1016/j.geoderma.2021.115111>
- Moore DC, Singer MJ (1990) Crust formation effects on soil-erosion processes. *Soil Sci Soc Am J* 54:1117–1123. <https://doi.org/10.2136/sssaj1990.03615995005400040033x>
- Moriwaki H, Inokuchi T, Hattanji T, Sassa K, Ochiai H, Wang G (2004) Failure processes in a full-scale landslide experiment using a rainfall simulator. *Landslides* 1:277–288. <https://doi.org/10.1007/s10346-004-0034-0>
- Okura Y, Kitahara H, Ochiai H, Sammori T, Kawanami A (2002) Landslide fluidization process by flume experiments. *Eng Geol*
- Regmi RK, Jung K, Nakagawa H, Do XK, Mishra BK (2017) Numerical analysis of multiple slope failure due to rainfall: based on laboratory experiments. *CATENA* 150:173–191. <https://doi.org/10.1016/j.catena.2016.11.007>
- Rieke-Zapp DH, Nearing MA (2005) Slope shape effects on erosion: a laboratory study. *Soil Sci Soc Am J* 69:1463–1471. <https://doi.org/10.2136/sssaj2005.0015>
- Song YX, Huang D, Cen DF (2016) Numerical modelling of the 2008 Wenchuan earthquake-triggered daguangbao landslide using a velocity and displacement dependent friction law. *Eng Geol* 215:50–68. <https://doi.org/10.1016/j.enggeo.2016.11.003>
- Sun P, Wang HJ, Wang G, Li RJ, Zhang Z, Huo XT (2021) Field model experiments and numerical analysis of rainfall-induced shallow loess landslides. *Eng Geol* 295. <https://doi.org/10.1016/j.enggeo.2021.106411>
- Tsai TL, Chen HE, Yang JC (2008) Numerical modeling of rain-storm-induced shallow landslides in saturated and unsaturated soils. *Environ Geol* 55:1269–1277. <https://doi.org/10.1007/s00254-007-1075-1>
- Tu XB, Kwong A, Dai FC, Tham LG, Min H (2009) Field monitoring of rainfall infiltration in a loess slope and analysis of failure mechanism of rainfall-induced landslides. *Eng Geol* 105:134–150. <https://doi.org/10.1016/j.enggeo.2008.11.011>
- Wang D, Li L, Li Z (2014a) A regularized lagrangian meshfree method for rainfall infiltration triggered slope failure analysis. *Eng Anal Boundary Elem* 42:51–59. <https://doi.org/10.1016/jenganabound.2013.09.001>
- Wang G, Sassa K (2001) Factors affecting rainfall-induced flowslides in laboratory flume tests. *Geotechnique* 51:587–599. <https://doi.org/10.1680/geot.51.7.587.51386>
- Wang GH, Zhang DX, Furuya G, Yang J (2014b) Pore-pressure generation and fluidization in a loess landslide triggered by the 1920 Haiyuan earthquake, China: a case study. *Eng Geol* 174:36–45. <https://doi.org/10.1016/j.enggeo.2014.03.006>
- Wang HH, Tuo XG, Zhang GY, Peng FL (2013) Panzhihua airport landslide (Oct. 3rd 2009) and an emergency monitoring and warning system based on the internet of things. *J Mountain Sci* 10:873–884. <https://doi.org/10.1007/s11629-013-2368-3>
- Wang JD, Xu YJ, Ma Y, Qiao SN, Feng KQ (2018) Study on the deformation and failure modes of filling slope in loess filling engineering: a case study at a loess mountain airport. *Landslides* 15:2423–2435. <https://doi.org/10.1007/s10346-018-1046-5>
- Wang JD, Zhang DF, Wang NQ, Gu TF (2019) Mechanisms of wetting-induced loess slope failures. *Landslides* 16:937–953. <https://doi.org/10.1007/s10346-019-01144-4>
- Wen BP, Wang S, Wang E, Zhang JM, Wu YG, Wang X (2005) Deformation characteristics of loess landslide along the contact between loess and neocene red mudstone. *Acta Geologica Sinica-English Edition* 79:139–151
- Wu LZ, Zhang LM, Zhou Y, Xu Q, Yu B, Liu GG, Bai LY (2018) Theoretical analysis and model test for rainfall-induced shallow landslides in the red-bed area of Sichuan. *Bull Eng Geol Environ* 77:1343–1353. <https://doi.org/10.1007/s10064-017-1126-0>
- Wu LZ, Zhou Y, Sun P, Shi JS, Liu GG, Bai LY (2017) Laboratory characterization of rainfall-induced loess slope failure. *CATENA* 150:1–8. <https://doi.org/10.1016/j.catena.2016.11.002>
- Yang KH, Thuo JN, Huynh VDA, Nguyen TS, Portelinha FHM (2018) Numerical evaluation of reinforced slopes with various backfill-reinforcement-drainage systems subject to rainfall infiltration. *Comput Geotech* 96:25–39. <https://doi.org/10.1016/j.compgeo.2017.10.012>
- Zhang CL, Li TL, Li P (2014a) Rainfall infiltration in Chinese loess by in situ observation. *J Hydrol Eng* 19:06014002. [https://doi.org/10.1061/\(ASCE\)HE.1943-5584.0001015](https://doi.org/10.1061/(ASCE)HE.1943-5584.0001015)
- Zhang FY, Shu HP, Yan BB, Wu XG, Lan HX, Peng JB (2023) Characteristic analysis and potential hazard assessment of reclaimed mountainous areas in Lanzhou, China. *Catena* 221. <https://doi.org/10.1016/j.catena.2022.106771>
- Zhang FY, Wang GH, Peng JB (2022) Initiation and mobility of recurring loess flowslides on the Heifangtai irrigated terrace in China:

- insights from hydrogeological conditions and liquefaction criteria. *Eng Geol* 302. <https://doi.org/10.1016/j.enggeo.2022.106619>
- Zhang FY, Wang GH, Kamai T, Chen WW, Zhang DX, Yang J (2013) Undrained shear behavior of loess saturated with different concentrations of sodium chloride solution. *Eng Geol* 155:69–79. <https://doi.org/10.1016/j.enggeo.2012.12.018>
- Zhang FY, Yan BB, Feng XM, Lan HX, Kang C, Lin XS, Zhu XH, Ma WG (2019a) A rapid loess mudflow triggered by the check dam failure in a bulldoze mountain area, Lanzhou, China. *Landslides* 16:1981–1992. <https://doi.org/10.1007/s10346-019-01219-2>
- Zhang J, Jiao JJ, Yang J (2000) In situ rainfall infiltration studies at a hillside in Hubei province, China. *Eng Geol AMSTERDAM*- 57. [https://doi.org/10.1016/S0013-7952\(99\)00126-X](https://doi.org/10.1016/S0013-7952(99)00126-X)
- Zhang JM, Luo Y, Zhou Z, Victor C, Duan MD (2021) Research on the rainfall-induced regional slope failures along the Yangtze River of Anhui, China. *Landslides* 18: 1801–1821. <https://doi.org/10.1007/s10346-021-01623-7>
- Zhang M, Liu J (2010) Controlling factors of loess landslides in western China. *Environ Earth Sci* 59:1671–1680. <https://doi.org/10.1007/s12665-009-0149-7>
- Zhang M, Yang L, Ren XW, Zhang CY, Zhang TL, Zhang JJ and Shi XY (2019b) Field model experiments to determine mechanisms of rainstorm-induced shallow landslides in the Feiyunjiang river basin, China. *Eng Geol* 262. <https://doi.org/10.1016/j.enggeo.2019.105348>
- Zhang S (2020) Research on failure mechanism and early warning model of loess high fill slope. Chengdu University of Technology. (in Chinese with English abstract)
- Zhang S, Zhang X, Pei X, Wang S, Huang R, Xu Q, Wang Z (2019c) Model test study on the hydrological mechanisms and early warning thresholds for loess fill slope failure induced by rainfall. *Eng Geol* 258. <https://doi.org/10.1016/j.enggeo.2019.05.012>
- Zhang Y, Li W, Song B, Zhang F (2014b) Instability mechanism of a large filled loess landslide in Dongxiang County, Gansu province. *Journal of Lanzhou University Natural Science* 50:484–489 (in Chinese with English abstract)
- Zhou Z, Zhang JM, Ning FL, Luo Y, Chong L, Sun KB (2020) Large-scale test model of the progressive deformation and failure of cracked soil slopes. *J Earth Sci* 31:1097–1108. <https://doi.org/10.1007/s12583-020-1342-6>

Springer Nature or its licensor (e.g. a society or other partner) holds exclusive rights to this article under a publishing agreement with the author(s) or other rightsholder(s); author self-archiving of the accepted manuscript version of this article is solely governed by the terms of such publishing agreement and applicable law.